Materials Today Communications 8 (2016) 156–164

Energy absorbing characteristics of the composite contoured-core sandwich panels

A.K. Haldar[a,*], J. Zhou[a], Z. Guan[a,b]

[a] School of Engineering, University of Liverpool, Liverpool L69 3GH, United Kingdom
[b] School of Mechanical Engineering, Chengdu University, Shiling, Chengdu, Sichuan, China

ARTICLE INFO

Article history:
Received 2 July 2016
Accepted 1 August 2016
Available online 4 August 2016

Keywords:
CFRP
GFRP
Contoured-core sandwich panels
Energy absorption

ABSTRACT

It is a challenging task to reduce the weight and manufacturing cost of a lightweight energy absorbing structure, while at the same time to maintain a reasonable strength and structural performance. This paper investigates the energy absorbing characteristics of the sandwich panels based on spherical-roof and flat-roof composite contoured cores subjected to quasi-static loading. Initial attention was focused on establishing the influence of the core profile and core cell wall thickness on the energy absorbing characteristics of both glass fibre reinforced plastic (GFRP) and carbon fibre reinforced plastic (CFRP) panels. It has been shown that the specific energy absorption capacity of the panel increases nonlinearly with increasing core cell wall thickness, with the spherical-roof cores outperforming their flat-roof counterparts. The results of these tests were compared with previously published data on a range of the relevant core structures, where it has been shown that the energy absorbing characteristics of the current spherical-roof system are superior to other core structures, such as aluminium and composite egg-box structures. Finally, a finite element analysis was undertaken to predict the crushing behaviour, energy absorbing characteristics and the failure modes of these core materials in reasonably good correlation with the corresponding test results.

1. Introduction

The superior energy absorption and crashworthiness properties of composite materials have increasingly attracted a lot of attention from a range of sectors, including those associated with the automotive and aerospace industry [1]. A number of studies have been undertaken to investigate the influence of core design, such as metallic foam, egg-box and cellular cores, on energy absorption [1–13]. Periodic cellular core structures can be formed by a repetition of a well-defined unit cell through an array that can be either two dimensional or three dimensional [2]. Amongst the variety of cellular cores currently available, it is interesting to study a cellular core or structure made up of an interconnected network of cells. Egg-box is one of such structures. Energy absorbing structure based on aluminium egg-box was introduced to understand its collapse mechanism [3]. Experiments suggested that egg-box structures deform by either the rotation of a stationary plastic hinge or by a travelling plastic knuckle, depending upon the in-plane kinematic constraints imposed upon the egg-box.

Chung et al. [4] fabricated composite egg-box structures and stated that their density, boundary conditions and geometry affected the energy absorption. Fibre volume fraction and fibre architecture were varied by changing the stacking sequence of the fabrics during the initial lay-up and draping. In these samples, two parameters, namely fibre volume fraction and fibre architecture, were modified to define the amount of energy absorbed by the core. The production of foam filled egg-box sandwiches via autoclave curing was explained by Yoo [5]. It consisted of draping the prepregs onto the lower half of a silicone rubber mould, closing with the upper half and vacuum bagging the tool with a breather fabric and a nylon film. The core was cured in an autoclave following a specific heating cycle. Flat composite sheets were then attached to the surfaces of the core using adhesive bonding, to create a sandwich panel. Moreover, a self-expanding foam with spraying gases was sprayed into the core, with its cavities being completely filled. The crushing behaviour, crushing force and energy absorption of the egg-box cells, which are essential for comprehensive designs and subsequent improvements, were analysed.

The deformation process of a spherical aluminium shell was studied by Oliveira et al. [6]. Here, thin and thick cells were analysed under compression load between rigid plates, simulating bonded and unbonded conditions. The effect of the boundary conditions of

* Corresponding author.
E-mail address: a.k.haldar@liv.ac.uk (A.K. Haldar).

http://dx.doi.org/10.1016/j.mtcomm.2016.08.002

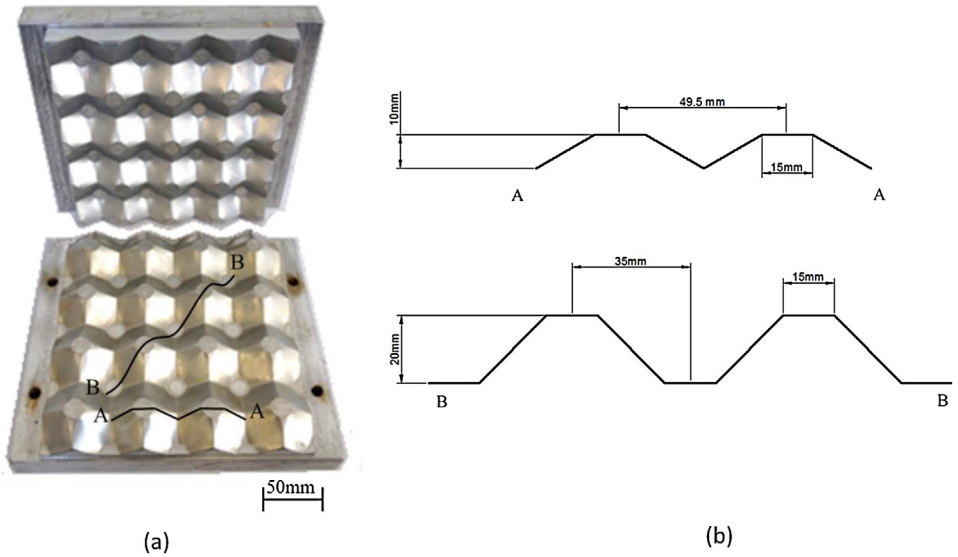

Fig. 1. Images of (a) aluminium flat-roof contoured moulds (egg box mould) and drawing of (b) cross section of the geometry.

egg-box was also studied by Nowpada et al. [7] through a comparison of the free-edge condition, finite number of cells and in situ constraints. It was found that the energy absorbed by the in situ constrained frustum is 80% greater than that separated from the egg-box panel with free edge boundary conditions.

Compression tests were performed and explained by Cartié [8] in his attempt to analyse the extension of fibre and resin properties on the panel characteristics. The main energy absorption mechanism was due to the extension of delamination, but additionally associated with tensile fibre breaking leading to a drop in load. Carrilo et al. [9] investigated a scaling effect that predicts response parameters based on compression tests. It was proven that the damage threshold energy varies with the scaling effect. Zhang et al. [10] described and explained the damage initiation and growth based on the load displacement curve obtained from the crushing test. The transitions of the specimen from an intact state to a damaged state were observed. As the crushing continues, different trends appear after the peak level leading to the main load decrease.

Although some work has been carried out to understand the effect of various sandwich geometries on energy absorption, there is limited work reported on contoured core sandwich panels made of composites. The present study investigates the properties of a range of flat-roof and spherical-roof contoured core sandwich panels made of carbon and glass fibre composites to improve the energy absorption for lightweight structures. The study was initially carried out to characterise the quasi-static response of these panels based on two geometries of contoured core. Furthermore, the specific energy absorption properties of these novel sandwich panels are compared with those offered by other types of core materials and designs. Finally, a finite element analysis was undertaken to predict the crushing behaviour, energy absorbing characteristics and the failure modes of these core materials, in a reasonably good agreement with the experimental results.

2. Experimental work

2.1. Core designs

Two types of core structures were investigated in this study. Initially, aluminium moulds shown in Fig. 1(a) were used to manufacture a series of flat-roof contoured cores. The cross section geometry of this contoured core mould is shown in Fig. 1(b). The design of flat-roof contoured panels are based on a same geometry described as egg-box panel by Zupan et al. [3] and Chung et al. [4]. A second design, based on a core with spherical caps, was also

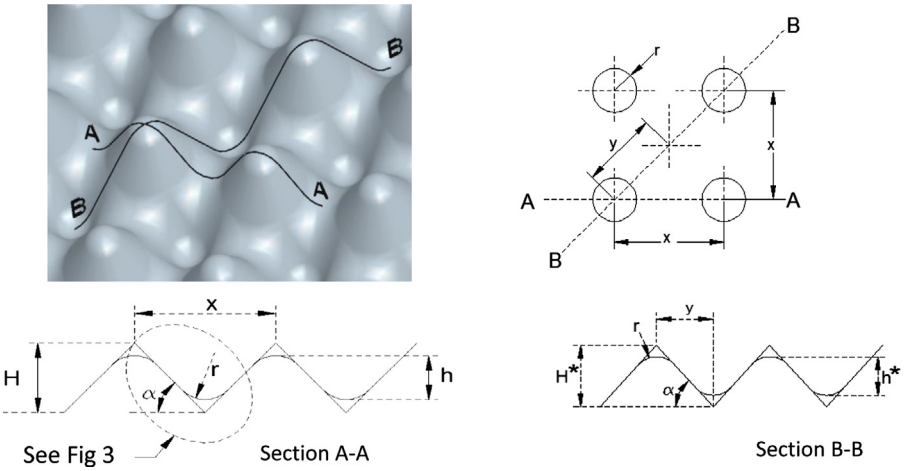

Fig. 2. Details of the design of the spherical-roof contoured core.

Table 1
Details of the glass fibre and carbon fibre reinforced epoxy composites [15].

Prepreg	Resin type	Resin content (%wt)	Fibre type	Weave style	Laminate density (kg/m^3)	Thickness of one ply cured (mm)	Curing temperature (°C)	Dwell time (Min)
GFRP	Epoxy	40 ± 3	E-Glass	Four Harness Satin	1750	0.1	145	90
CFRP	Epoxy	53 ± 3	3k HTA	Plain	1390	0.25	120	90

fabricated using different aluminium moulds. This design is not symmetrical, having the upper and lower halves that are a combination of two different profiles as shown in Fig. 2. A more detailed description of this cell geometry is shown in Fig. 3. In Fig. 2, Section A-A, r is the radius of the curvature, this being 4 mm in the current design, α is the angle of the cell walls (50° in the present case), H is the effective height, and h is the height of the contoured section.

The value of the height of the contour can be found from:

$$h = H - 2l \tag{1}$$

where l is the distance between the effective height and the top of the spherical, as shown in Fig. 3. The actual height of the core is defined as:

$$h = x\frac{\tan\alpha}{2} + 2r\left(1 - \frac{1}{\cos\alpha}\right) \tag{2}$$

where x is the distance between the centres of two adjacent domes.

Now, considering Section B-B in Fig. 2, the radius and slope of the cell are same as those in Section A-A. However, the extended and actual heights are different, which are expressed by H^* and h^* as:

$$h^* = H^* - 2l \tag{3}$$

$$h^* = x\frac{\tan\alpha}{\sqrt{2}} + 2r\left(1 - \frac{1}{\cos\alpha}\right) \tag{4}$$

The calculated actual heights h and h^* for Section A-A and B-B are 7.5 mm and 12.5 mm, respectively.

2.2. Manufacture of the cores

The above-mentioned cores were manufactured by using glass fibre reinforced plastic (GFRP) or carbon fibre reinforced plastic (CFRP), details of which are given in Table 1. Individual sheets of prepreg were cut from continuous rolls and laid in moulds. A release agent (CILRelease 1711E supplied by CIL-Bond) was sprayed on the interior surfaces of the moulds to ensure easy demoulding at the end of the cure cycle. The GFRP cores were manufactured by stacking 5, 10 and 15 prepreg plies in the moulds, yielding nominal thicknesses for the cores of 0.5, 1.0 and 1.5 mm. CFRP cores having the similar nominal thicknesses were produced by stacking 2, 4 and 6 prepreg plies in the moulds. The aluminium moulds were then placed in a hot press and cured according to the manufacturer's specifications (Table 1).

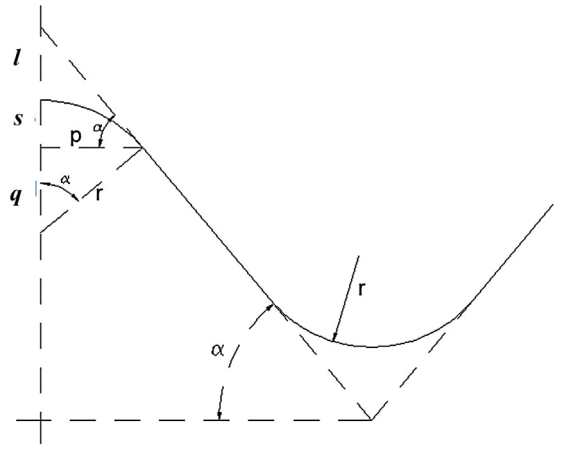

Fig. 3. Detailed design of the spherical-roof cell.

2.3. Bonding between skin and core

Composite skins, based on either CFRP or GFRP according to the core material, were bonded to the core using a two-part epoxy resin (Araldite 420 A/B) supplied by Easy-Composites. The nominal skin thickness was 0.5 mm. The adhesive was cured in an oven at 120 °C for approximately one hour.

2.4. Quasi-static compression

The specimens were subjected to quasi-static compression using an Instron 4505 universal test machine. Testing was initially conducted on 2 × 2 cell (i.e. 100 × 100 mm), then flat-roof contoured panels, followed by 3 × 3 cell (i.e. 60 × 60 mm) spherical-roof panels. All the tests were undertaken at a crosshead displacement rate of 1 mm/min and the testing was interrupted when the panel was fully crushed. At least three tests were carried out for each sample type. Compression stress-strain curves were calculated from the applied force (normalised by the planar area of the samples) and the crosshead displacement (normalised by the original height of the samples).

3. Finite element modelling

Finite element models were developed to simulate the crushing behaviour of these contoured sandwich panels subjected to quasi-static compression.

3.1. Mesh generation, boundary and loading conditions

Fig. 4 shows the finite element mesh of a contoured core based sandwich panels. Here, the contoured cores were meshed using six-noded triangular solid elements, while the skins using eight-noded brick elements. The loading platens above and below the

Table 2
Properties of the woven fabric glass-fibre reinforced plastic, (GFRP) and the woven fabric carbon-fibre reinforced plastic, (CFRP) [15].

Symbol	GFRP	CFRP	Property
E_1^o [GPa]	23	48	Young's modulus in longitudinal direction
E_2^o [GPa]	23	48	Young's modulus in transverse direction
E_3^o [GPa]	5	1	Young's modulus in thickness direction
υ_{12}^o	0.15	0.1	Poisson's ratio in 1–2 plane
υ_{13}^o	0.15	0.1	Poisson's ratio in 1–3 plane
υ_{23}^o	0.15	0.1	Poisson's ratio in 2–3 plane
G_{12}^o [GPa]	5	9	Shear modulus in 1–2 plane
G_{13}^o [GPa]	5	9	Shear modulus in 1–3 plane
G_{23}^o [GPa]	5	9	Shear modulus in 2–3 plane
σ_{1t}^r [MPa]	320	550	Longitudinal tensile strength
σ_{1c}^r [MPa]	260	150	Longitudinal compression strength
σ_{2t}^r [MPa]	320	550	Transverse tensile strength
σ_{2c}^r [MPa]	260	150	Transverse compressive strength
σ_{12}^r [MPa]	100	120	Shear strength in 1–2 plane
σ_{13}^r [MPa]	100	120	Shear strength in 1–3 plane
σ_{23}^r [MPa]	100	120	Shear strength in 2–3 plane

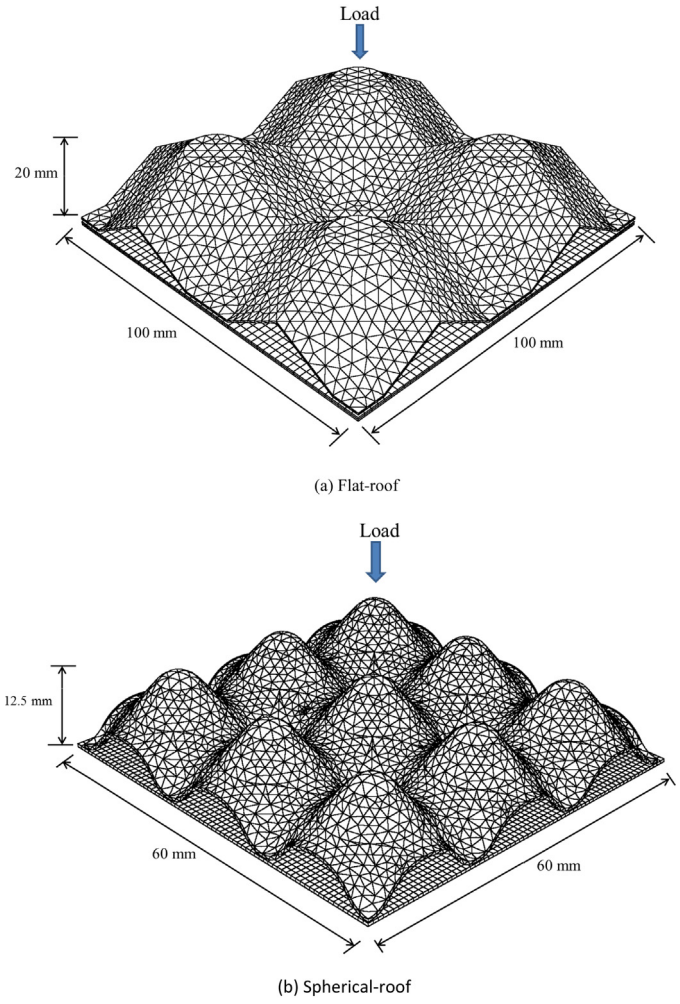

Fig. 4. The geometry, mesh, boundary and loading conditions of contoured core based sandwich panels.

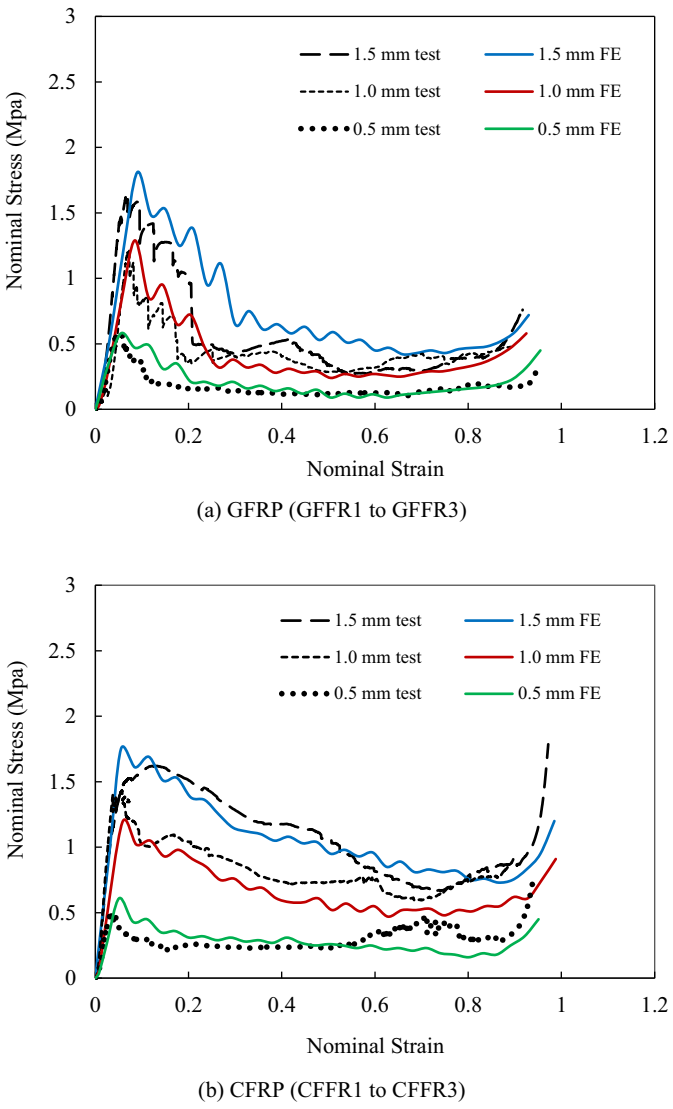

Fig. 5. Quasi-static stress-stain traces of flat-roof contoured panels based on various wall thicknesses of the core cell.

panel were meshed using rigid surface elements. The model has a number of interfaces that need to be considered. These include those between the contoured core and skin, those between the skin and platen, as well as those between the composite contoured core and the platen. The platens are allowed to contact the contoured core in case the skin is damaged. Material properties of GFRP and CFRP composite cores are presented in Table 2, respectively.

3.2. Modified 3D Hashin's failure criteria

The Hashin's failure criteria for fibre reinforced composites are available in ABAQUS, however they are limited to apply for 2D cases, i.e. using shell or continuum shell elements. Therefore, in order to capture failure through its thickness, the modified Hashin's 3D failure criteria[11] are assigned into ABAQUS/Explicit using a user-defined subroutine [12]. Those modified 3D failure criteria in contoured-core sandwich can be defined in the (1, 2, 3) coordinate system as given below:

Tension failure in warp and weft fibre direction:

$$\sigma_{11} > 0, f_{1t} = \left(\frac{\sigma_{11}}{\sigma_{1t}^r}\right)^2 + \left(\frac{\sigma_{12}}{\sigma_{12}^r}\right)^2 + \left(\frac{\sigma_{13}}{\sigma_{31}^r}\right)^2 - 1 \geq 0 \quad (5)$$

$$\sigma_{22} > 0, f_{2t} = \left(\frac{\sigma_{22}}{\sigma_{2t}^r}\right)^2 + \left(\frac{\sigma_{12}}{\sigma_{12}^r}\right)^2 + \left(\frac{\sigma_{23}}{\sigma_{23}^r}\right)^2 - 1 \geq 0 \quad (6)$$

Compression failure in the warp ($i=1$) and weft ($i=2$) fibre direction and through-the-thickness ($i=3$) crush failure:

$$\sigma_{ii} < 0, f_{ic} = \left(\frac{\sigma_{ii}}{\sigma_{ic}^r}\right)^2 - 1 \geq 0 \quad (7)$$

In-plane shear failure:

$$f_{12} = \left(\frac{\sigma_{12}}{\sigma_{12}^r}\right)^2 - 1 \geq 0 \quad (8)$$

In Eqs. (5)–(8), σ_{ij}^r ($i, j = 1t, 1c, 2t, 2c, 12, 23, 31$) are the material strengths (Table 2). The progressive damage models for composites are based on the degradation of the material stiffness, whose non-zero matrix components can be expressed as:

$$\begin{aligned} C_{11} &= (1-d_1)E_1^0(1-(1-d_2)(1-d_{3c})\upsilon_{23}^0\upsilon_{32}^0)\Omega \\ C_{22} &= (1-d_2)E_2^0(1-(1-d_1)(1-d_{3c})\upsilon_{13}^0\upsilon_{31}^0)\Omega \\ C_{33} &= (1-d_{3c})E_3^0(1-(1-d_1)(1-d_2)\upsilon_{12}^0\upsilon_{21}^0)\Omega \end{aligned} \quad (9a)$$

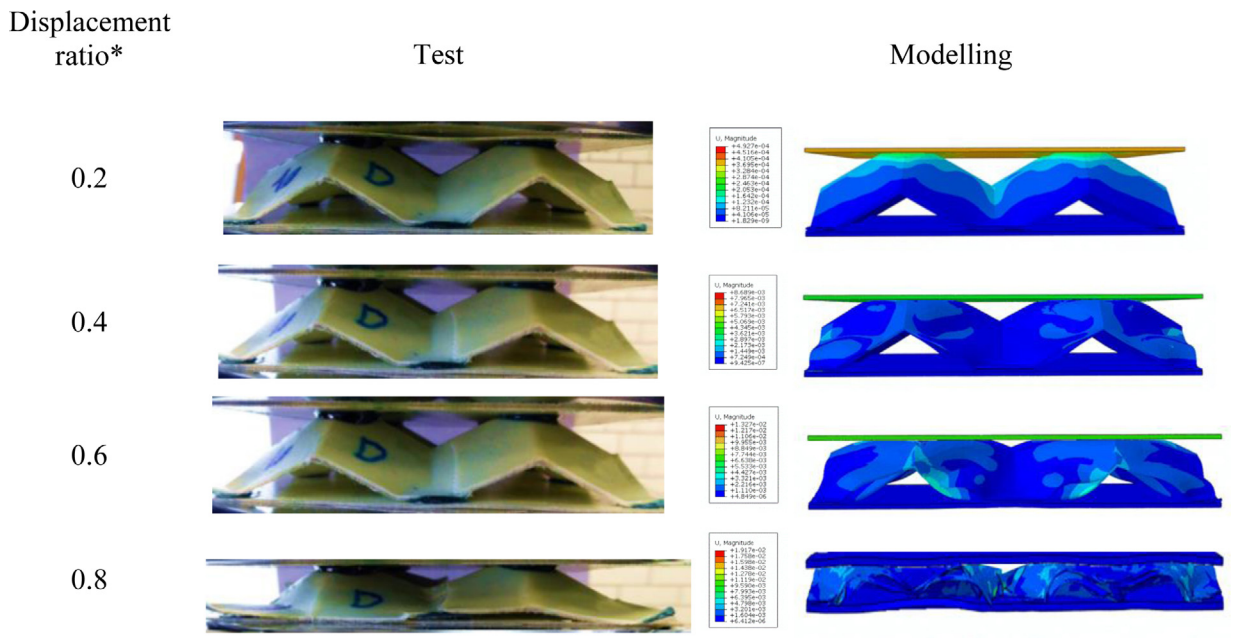

Fig. 6. Various level of deformation in the flat-roof glass fibre contoured panel (GFFR1) during compression (*displacement ratio = displacement/the original height of the core).

$$C_{12} = (1-d_1)E_1^0((1-d_2)\upsilon_{21}^0 - (1-d_2)(1-d_{3c})\upsilon_{31}^0\upsilon_{23}^0)\Omega$$
$$C_{23} = (1-d_2)E_2^0((1-d_{3c})\upsilon_{32}^0 - (1-d_1)(1-d_{3c})\upsilon_{12}^0\upsilon_{31}^0)\Omega \quad (9b)$$
$$C_{13} = (1-d_1)E_1^0((1-d_2)\upsilon_{31}^0 - (1-d_2)(1-d_{3c})\upsilon_{21}^0\upsilon_{32}^0)\Omega$$
$$C_{21} = (1-d_2)E_2^0((1-d_1)\upsilon_{12}^0 - (1-d_1)(1-d_{3c})\upsilon_{13}^0\upsilon_{32}^0)\Omega$$
$$C_{31} = (1-d_{3c})E_3^0((1-d_1)\upsilon_{13}^0 - (1-d_1)(1-d_2)\upsilon_{12}^0\upsilon_{23}^0)\Omega \quad (9c)$$
$$C_{32} = (1-d_{3c})E_3^0((1-d_2)\upsilon_{23}^0 - (1-d_1)(1-d_{3c})\upsilon_{31}^0\upsilon_{13}^0)\Omega$$
$$C_{44} = (1-d_{12})G_{12}^o$$
$$C_{55} = (1-d_2)G_{23}^o \quad (9d)$$
$$C_{66} = (1-d_1)G_{13}^o$$

where the di are the damage variables, namely, d_1 and d_2 correspond to the failure in warp and weft fibre directions, respectively, d_{3c} describes through-the-thickness composite crushing failure, and d_{12} refers to the in-plane shear failure. Here, d_1 and d_2 take different values at tension and compression and are defined as:

$$d_1 = 1-(d_{1t})(1-d_{1c})$$
$$d_2 = 1-(d_{2t})(1-d_{2c}) \quad (9e)$$

Also

$$\Omega = 1/(1-\nu_{12}^o\nu_{21}^o - \nu_{23}^o\nu_{32}^o - \nu_{13}^o\nu_{31}^o - 2\nu_{21}^o\nu_{32}^o\nu_{13}^o) \quad (9f)$$

In the equations above, the subscripts "t" and "c" denote tensile and compressive failure, respectively, E_i^o, υ_{ij}, $G_{ij}(i=1,2,3)$ are the Young's moduli, shear moduli and Poisson's ratios of the virgin composite material, which can be found in Table 2. Moreover, in order to ensure symmetry of the stiffness matrix, the Poisson's ratios need to satisfy the following conditions, i.e.

$$\frac{\upsilon_{12}^o}{E_1^o} = \frac{\upsilon_{21}^o}{E_2^o}, \frac{\upsilon_{23}^o}{E_2^o} = \frac{\upsilon_{32}^o}{E_3^o}, \frac{\upsilon_{13}^o}{E_1^o} = \frac{\upsilon_{31}^o}{E_3^o} \quad (10)$$

3.3. Implementation of the material model in ABAQUS/Explicit

The material model and the previously mentioned failure criteria in ABAQUS/Explicit were implemented using the user-defined VUMAT subroutine. This subroutine is called for each iteration. This enables ABAQUS/Explicit to acquire the necessary information according to the state of the material and its mechanical response at each integration point within each element. A series of numerical studies with different durations were conducted for finding the appropriate time step which results in negligible dynamic effects. The suitable time step in this analysis was found to be 0.1 s. Hashin's 3D failure criteria are introduced as given in Eqs. (5)–(8). The given material stiffness coefficients are used to calculate the stresses within the VUMAT subroutine. The failed element is removed from the mesh when the failure criteria are satisfied to all integration points within an element. By this way the model stiffness in the subsequent deformation is not resisted by the stress of the element.

3.4. Cohesive elements and material properties

Cohesive elements which are available in ABAQUS, were used to model the resin layer located at the interface between the skins and core [13]. Traction-separation model defines elastic response by assuming an initially linear elastic behaviour at the beginning phase, later followed by damage evolution. Elastic constitutive matrix represents the elastic behaviour of the element. Here, the true thickness of the cohesive layer (t_c) should be used to determine the diagonal terms in the elasticity matrix as follows:

$$K_{nn} = \frac{E_n}{t_c}, K_{ss} = \frac{E_s}{t_c}, K_{tt} = \frac{E_t}{t_c} \quad (11)$$

where E_n denotes stiffness along the normal direction, while E_s and E_t along the tangential directions. The damage initiation and damage evolution of cohesive layer were simulated by quadratic nominal stress and energy criterion, respectively. When a quadratic interaction function, involving the nominal stress ratios reaches unity, it leads to damage initiation. Energy in conjunction with a linear softening law forms damage evolution. The mechanical properties of the cohesive elements were obtained from [14].

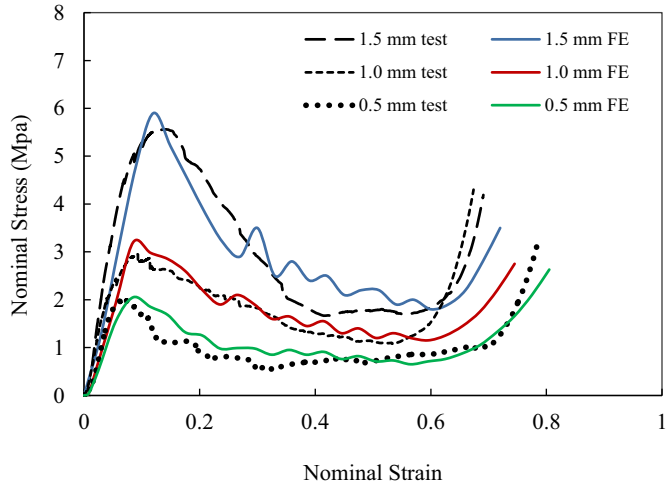

(a) GFRP (GFSR1 to GFSR3)

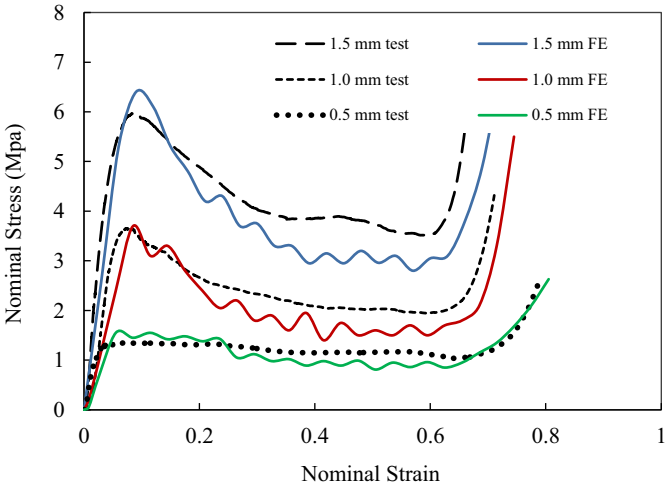

(b) CFRP (CFSR1 to CFSR3)

Fig. 7. Quasi-static stress-stain traces of spherical-roof contoured panels based on various wall thicknesses of the core cell.

4. Results and discussion

4.1. Quasi-static compression on contoured sandwich panels

Fig. 5 shows stress-strain traces following tests on 2 × 2 flat-roof cores with cell wall thicknesses of 0.5, 1.0 and 1.5 mm. The curves for the GFRP materials exhibit a brittle mode of failure, with higher peak stresses for the thicker samples, as shown in Fig. 5(a). At the initial peak stress, cracks were initiated and propagated with continued loading, causing a reduction in the structural stiffness. The cone then started to buckle, leading to a sudden drop in stress. The cell walls subsequently debonded from the skins, resulting in a plateau region between strains of 0.1 and 0.5. During the later stages of the test, the sample was completely crushed and the stress started to increase rapidly, as shown in deformation modes in Fig. 6. This is effectively the densification threshold of the structure, which was found to occur at strains between 0.6 and 0.8, in the traces in Fig. 5(a). Tests on the CFRP panels indicated that they failed in a progressive manner, resulting in a relative mild decline in the stress-strain curves, Fig. 5(b). Here, the densification occurred at strains in a range of 0.7–0.9, indicating the CFRP panels having a delayed densification threashold.

Table 3
Summary of the experimental and numerical peak stresses.

Specimen ID	Thickness of the cell wall (mm)	Maximum Peak (Experimental)	Maximum Peak (FE)
GFFR1	0.5	0.49	0.57
GFFR2	1.0	1.29	1.21
GFFR3	1.5	1.59	1.80
CFFR1	0.5	0.51	0.60
CFFR2	1.0	1.31	1.20
CFFR3	1.5	1.75	1.62
GFSR1	0.5	1.85	2.05
GFSR2	1.0	2.90	3.18
GFSR3	1.5	5.55	5.90
CFSR1	0.5	1.39	1.55
CFSR2	1.0	3.70	3.80
CFSR3	1.5	5.90	6.40

Compression tests were then performed on 3 × 3 cell spherical-roof contoured structures. During these tests, both the GFRP and CFRP panels responded in a linear elastic manner up to the peak stress, as shown in Fig. 7(a) and (b) respectively. The response then becomes nonlinear and the stress begins to decrease progressively as the specimen flattens between the plattens, with cracks and fibre fracture occurring within the structure. Similar to the flat-roof, the stress was rapidly increased in spherical-roof panels, with increasing cell wall thicknesses. For example, the maximum compressive stress exhibited on the 1.5 mm GFRP contoured sandwich panel is approximately three times of that of the 0.5 mm thick panel. The traces for the thicker CFRP panels drop gradually, stabilising at a significantly higher plateau level than the GFRP counterparts. Although the peak stress for the 0.5 mm GFRP panel based on five plies was higher than that of its CFRP counterpart, the subsequent plateau stress was much lower. This is likely due to the brittle nature of the failure, as well as occurrence of delamination between the plies.

4.2. Numerical modelling of the compression response of flat-roof and spherical-roof contoured cores

Figs. 5 and 7 also include the predicted stress-strain traces for the flat-roof and spherical-roof contoured cores based on the GFRP and CFRP, by the finite element models. The key features such as initial stiffness, peak stress, plateau and densification stages being captured with very good correlation between the experimental data and the numerical prediction. FE models can be used to estimate the energy absorption up to the densification stages. The predicted traces for all three cell wall thicknesses exhibit a fine agreement in the succeeding plateau stages. The cores with the thickest cell wall made from both the GFRP and the CFRP contribute a slightly higher peak stress in finite element models as compared to the experimental results. This may be associated with a slight variation on the wall thickness which is not considered in modelling. A summary of the experimental and numerical peak stresses is given in Table 3.

The progressive failure modes predicted were compared with those captured experimentally, which indicates reasonable correlation for specimens subjected to various levels of deformation, as shown in Fig. 6. Fig. 8(a) and (b) display a completely crushed sample and model with their skins removed. Clearly, the main characteristics of the experimental failure modes are captured in the model, in which flattening of the flat-roof contoured core and their final collapse are depicted here.

The progressive failure modes predicted in the spherical-roof core are shown in Fig. 9. The skins were also removed to assist viewing the progressive deformations. Clearly, the GFRP samples exhibited a brittle failure, involving extensive crushing and matrix cracking with fibre fracture. Again, the matrix cracking observed

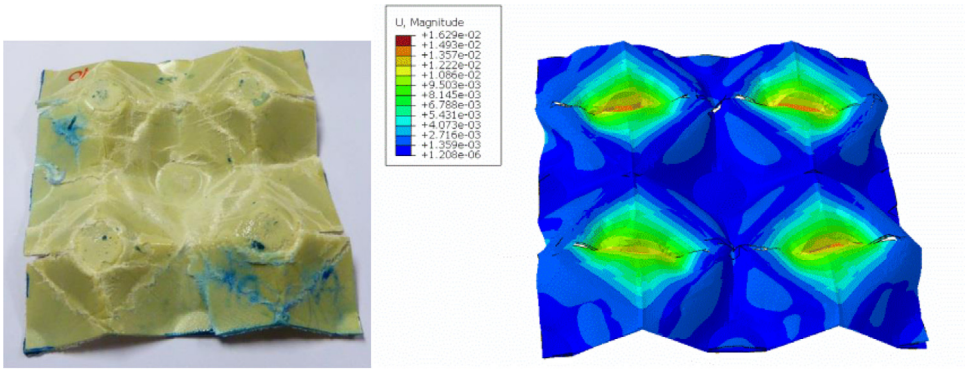

Fig. 8. Ultimately collapesed flat-roof contoured core (GFFR1) (legend in meter).

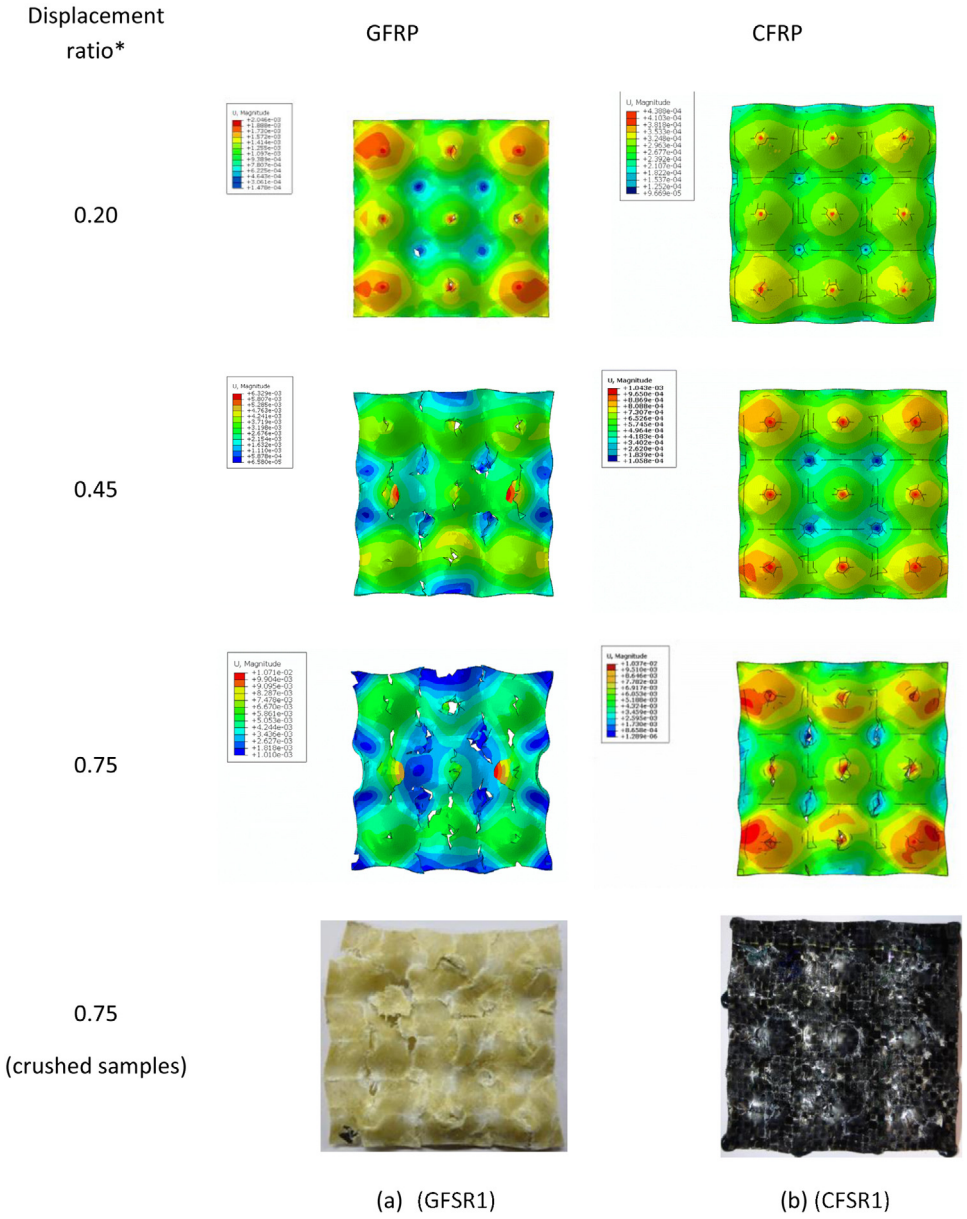

Fig. 9. Crushed core of spherical-roof contoured panels (*displacement ratio = displacement/the original height of the core).

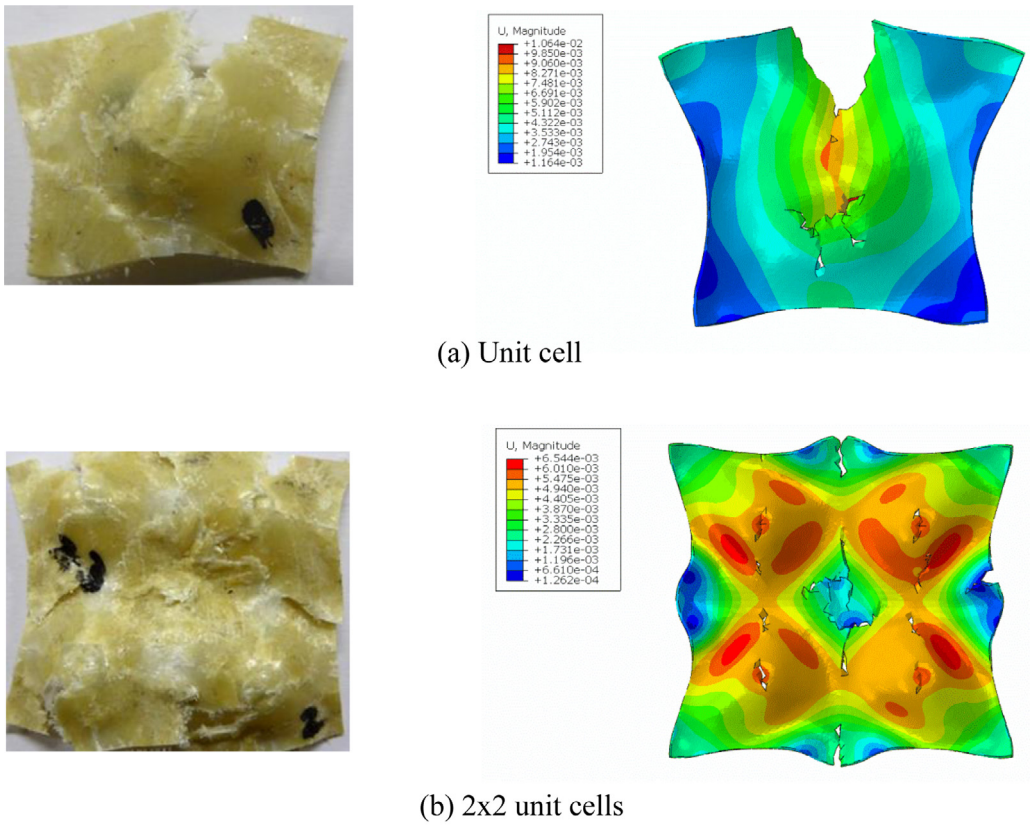

Fig. 10. Comparison of the GFRP spherical-roof cores predicted by the numerical model with the experimental samples.

in the finally collapsed GFRP sample is reproduced by the finite element simulations, as shown in Fig. 9(a). On the contrary, the CFRP panels were failed in a ductile manner with the core almost flattened with matrix cracking, Fig. 9(b).

Further, numerical modelling of a unit cell and 2×2 unit cells made of GFRP was carried out on these spherical-roof contoured cores to provide more comparisons of the experimental failure mode and the simulated one. Fig. 10(a) and (b) show such comparisons, which clearly indicates that the numerical model provides the reasonably good predictions of the failure modes.

4.3. Comparison of the current contoured core panels with other energy-absorbing cores

In addition, since mass is a critical parameter when designing energy absorbers destined for use in weight-sensitive applications, the specific energy absorption (SEA) was used in this study to characterise the response of the panels. The *SEA* can be defined as:

$$SEA = \frac{\int_0^{\delta_{max}} \sigma(\delta) d\delta}{\rho \overline{\rho}} \tag{12}$$

where σ is the stress, δ is the nominal strain and δ_{max} is the nominal densification strain. To make a comparison with the energy absorption of aluminium and composite egg-box panels [3,5], the value of δ_{max} was chosen up to a nominal strain of 0.6 in the current study. ρ and $\overline{\rho}$ are the mass density of the solid material for composite cores and the relative density associated with each material system, which is defined as a mass of the panel divided by the mass of a solid rectangular block of the same material enclosing the core. The mass of the skin was eliminated from the calculations [5].

The SEA of the core structures was determined and the resulting values of the quasi-static specific energy absorption are presented in Fig. 11. Here, it is clearly highlighted that the SEA value increases with the cell wall thickness. For example, the average SEA value for the CFRP spherical-roof with the thickness of 1.5 mm was approximately 10.95 kJ/kg, compared to 0.5 mm thick one, which is around 8.37 kJ/kg (Fig. 11). These differences are even greater for the GFRP structures, which show that the 1.5 mm thick cell wall has a value of 8.07 kJ/kg, being over sixty percent greater than its 0.5 mm thick cell wall value. The predicted energy absorption using the FE models has also shown a good agreement with the experimental values.

The SEA of the current contoured panels was also compared with bonded aluminium egg-box [3] and the best energy absorbing

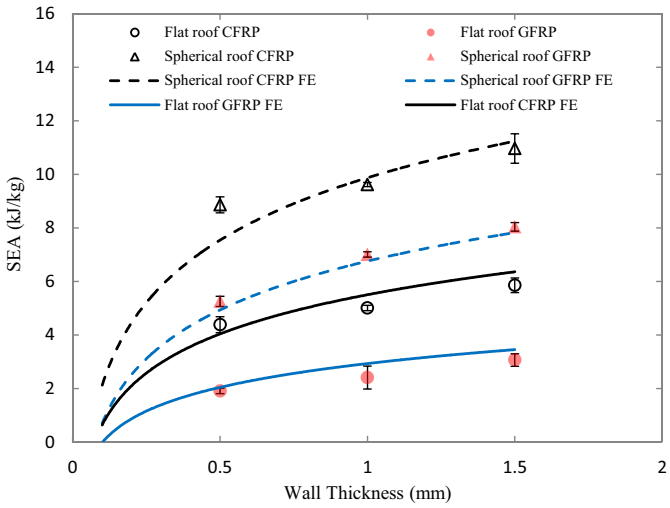

Fig. 11. Specific energy absorption of Spherical-roof and Flat-roof contoured structures made of CFRP and GFRP preprages.

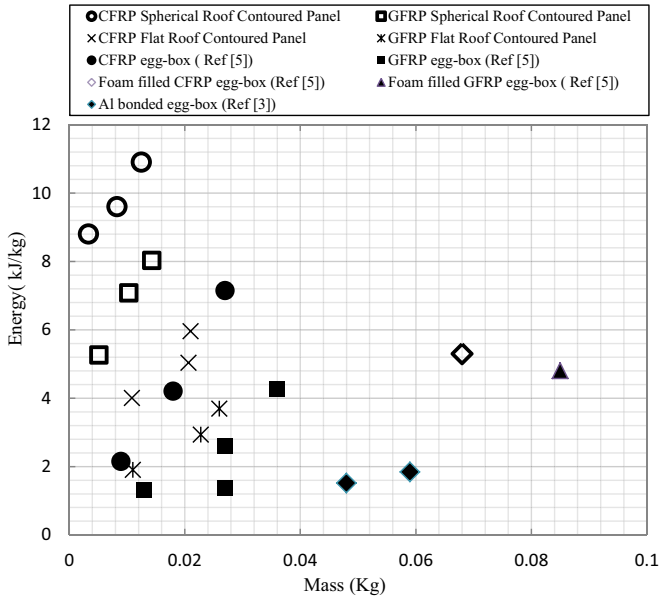

Fig. 12. Energy absorption per unit mass of the current panels and data from the literature.

systems from the reference [5], and the results are summarised as a function of mass in Fig. 12. In general, the spherical-roof panels offer excellent energy absorbing capacities, with values being up to ten times greater than the corresponding aluminium egg-box panels. Further, the spherical-roof panels are 50–60 percent better than the existing composite egg box panels in terms of SEA.

Relative to the other panels, the higher energy absorption capacities of these spherical-roof contoured panels are likely to be associated with the progressive failure mechanisms of the fibre and matrix in the cap region. Chung et al. [4] observed that the initial cracking in egg-box panels occurred at the circular perimeters of the upper and lower surfaces that are in contact with the plates/skins, as a result of the stress concentration there. However, no such regions of weakness exist in the spherical-roof, which may explain the great improvement in the structural performance. In addition, reducing the inner peak distance and the cell diameter gives a high density of cones throughout the structure, which results in an increased stiffness, hence, a higher stress level. This, in turn, improves the energy absorption capability of the spherical-roof contoured panels.

5. Conclusions

The energy-absorbing characteristics of contoured composite panels based on glass and carbon fibre reinforced epoxy have been evaluated at quasi-static loading. The peak stress and specific energy absorption of the core increase rapidly with increasing cell wall thickness. For a given material, the spherical-roof contoured panels out-perform their flat-roof counterparts with a higher stiffness and the plateau stresses, resulting in a higher level of energy absorption.

The performance of these panels is compared with the relevant existing designs such as egg-box panels based on aluminium, GFRP and CFRP, where it has been shown that the current spherical-roof composite designs offer excellent levels of energy absorption per unit mass, relative to egg-box type structures.

The predictions offered by the numerical models are found to be in a reasonably good agreement with the experimental data. The user-defined subroutine with the failure criteria has been successfully implemented into the material model in ABAQUS/Explicit to simulate the structural response of the current contoured cores. The validated models are ready to be used for further parametric studies to assist designing any new contoured core structures.

Acknowledgements

The authors are grateful to the university of Liverpool and Indian Government for the Research Studentship (A.K. Haldar).

References

[1] R. Alia, W. Cantwell, G. Langdon, S. Yuen, G. Nurick, The energy-absorbing characteristics of composite tube-reinforced foam structures, Compos. B: Eng. 61 (2014) 127–135.
[2] H.N. Wadley, Multifunctional periodic cellular metals, philosophical transactions of the royal society A: mathematical, Phys. Eng. Sci. 364 (2006) 31–68.
[3] M. Zupan, C. Chen, N. Fleck, The plastic collapse and energy absorption capacity of egg-box panels, Int. J. Mech. Sci. 45 (2003) 851–871.
[4] J. Chung, S. Chang, M. Sutcliffe, Deformation and energy absorption of composite egg-box panels, Compos. Sci. Technol. 67 (2007) 2342–2349.
[5] S. Yoo, S. Chang, M. Sutcliffe, Compressive characteristics of foam-filled composite egg-box sandwich panels as energy absorbing structures, Compos. A: Appl. Sci. Manuf. 41 (2010) 427–434.
[6] J.G. De Oliveira, T. Wierzbicki, Crushing analysis of rotationally symmetric plastic shells, J. Strain Anal. Eng. Des. 17 (1982) 229–236.
[7] S. Nowpada, E.C. Chirwa, P. Myler, E. Matsika, Aluminum egg-box panel as an energy absorber for pedestrian protection, Adv. Eng. Mater. 12 (2010) 591–595.
[8] D. Cartie, P. Irving, Effect of resin and fibre properties on impact and compression after impact performance of CFRP, Compos. A: Appl. Sci. Manuf. 33 (2002) 483–493.
[9] J. Carrillo, W.J. Cantwell, Scaling effects in the low velocity impact response of fiber-metal laminates, J. Reinf. Plast. Compos. (2008).
[10] D. Zhang, Y. Sun, L. Chen, N. Pan, A comparative study on low-velocity impact response of fabric composite laminates, Mater. Des. 50 (2013) 750–756.
[11] Z. Hashin, Failure criteria for unidirectional fiber composites, J. Appl. Mech. 47 (1980) 329–334.
[12] T.P. Vo, Z. Guan, W. Cantwell, G. Schleyer, Modelling of the low-impulse blast behaviour of fibre–metal laminates based on different aluminium alloys, Compos. B: Eng. 44 (2013) 141–151.
[13] Abaqus/Explicit, Abaqus analysis user's manual, Abaqus 6.12 HTML documentation, (2012).
[14] D. Karagiozova, G. Langdon, G. Nurick, S.C.K. Yuen, Simulation of the response of fibre–metal laminates to localised blast loading, International, J. Impact Eng. 37 (2010) 766–782.
[15] M. Rejab, W. Cantwell, The mechanical behaviour of corrugated-core sandwich panels, Compos. B: Eng. 47 (2013) 267–277.